PHYSICS AND CHEMISTRY OF SOLID STATE
V. 23, No. 1 (2022) pp. 77-88
Section: Chemistry

DOI: 10.15330/pcss.23.1.77-88

Vasyl Stefanyk Precarpathian National University

ФІЗИКА І ХІМІЯ ТВЕРДОГО ТІЛА
Т. 23, № 1 (2022) С.77-88
Хімічні науки

UDC: 549.731.13 ISSN 1729-4428

N. Danyliuk, S. Lischynska, T. Tatarchuk, V. Kotsyubynsky, V. Mandzyuk

Magnetite Nanoparticles Synthesized Using Grape Fruit Extract: Synthesis, Morphology, Hyperthermia Application and Catalytic Activity in Hydrogen Peroxide Decomposition

Vasyl Stefanyk Precarpathian National University, Ivano-Frankivsk, Ukraine, danyliuk.nazariy@gmail.com

The paper presents a simple one-step "green" approach to the synthesis of magnetite nanoparticles. The magnetite nanoparticles were synthesized using fruit extract obtained from grape peels and grape pulp. The formation of magnetite nanoparticles was confirmed by X-ray diffraction analysis (XRD), infrared spectroscopy (IR), Mössbauer spectroscopy, scanning electron microscopy (SEM) and energy dispersive spectroscopy (EDS). The crystallites sizes of magnetite nanoparticles are 7 and 14 nm for Fe_3O_4-peel and Fe_3O_4-pulp samples, respectively. Scanning electron microscopy images show that the samples consist of agglomerated nanoparticles. The synthesized magnetite nanoparticles showed good prospects for their use in magnetic hyperthermia. SAR values of 0.488 W/g and 1.330 W/g for Fe_3O_4-peel and Fe_3O_4-pulp samples, respectively. The maximum hyperthermia temperatures are 42.28 °C and 42.48 °C for Fe_3O_4-peel and Fe_3O_4-pulp samples, respectively. Studies of the catalytic activity of magnetite were performed in decomposition of hydrogen peroxide in a batch mode. The high catalytic activity of the synthesized samples makes them promising candidates for the decomposition of hydrogen peroxide in wastewater disinfection.

Keywords: green synthesis, magnetite, magnetic hyperthermia, catalytic activity, hydrogen peroxide.

Received 13 October 2021; Accepted 8 February 2022.

Introduction

There are three most common natural iron oxides: hematite α-Fe_2O_3, maghemite γ-Fe_2O_3, magnetite Fe_3O_4. Hematite Fe_2O_3 can exist in three structural modifications – α-, γ-, δ-Fe_2O_3, which have different properties depending on the synthesis method. Magnetite Fe_3O_4 belongs to the class of spinel compounds. Maghemite γ-Fe_2O_3 also has a spinel structure, but it contains cationic vacancies in the octahedral sublattice. Iron oxides are of great importance and widely used in catalysis [1, 2], biomedicine [3, 4], adsorption [5], photocatalysis [6, 7] etc. Fe_2O_3 is used as a catalyst in the extraction of ammonia, as a component of ceramics, as a dye for cements and paints, as a carrier of analog and digital information [8]. Due to its magnetic properties, magnetite is also used for targeted drug delivery in the magnetic hyperthermia and in magnetic resonance imaging for the diseases diagnostics [9]. Maghemite nanoparticles are also used in biomedicine because they are biocompatible and non-toxic to humans [10].

Magnetite forms the cubic crystals (spinel structure), the space group is Fd3m, the cell parameter a = 0.8397 nm, Z = 8. The crystal structure is a framework consisting of tetrahedral and octahedral groups formed by oxygen ions, in which the ferrous (Fe^{2+}) and ferric (Fe^{3+}) ions are placed. Magnetite is inversed spinel: tetrahedral positions are fully occupied by ferric ions, while octahedral positions are occupied by equal amounts of ferrous and ferric ions. Magnetite is usually non-stoichiometric. In such case, it has a cation-deficient octahedral sublattice. In stoichiometric magnetite, the ratio Fe^{2+}/Fe^{3+} is equal 0.5.

Table 1.

Characteristics of Fe_3O_4 nanoparticles obtained using different parts of plants.

Plant / part of a plant	Particle size, nm	Particle morphology	Refs.
Soybean sprouts	~8	Spherical	[18]
Aloe vera	~97-227	Spherical	[19]
Grape seeds	~30	Irregular shape	[20]
Papaya leaves	~33	Agglomerated lamellar structure with coarse grains and capsules	[21]
Green tea leaves	~4-6	Spherical	[22]
Lemon	~14-17	Spherical	[23]
Potato	~40	Cubic	[16]

Magnetite can be obtained by various methods, including co-precipitation [11], sol-gel method [12], microemulsion method [13], thermal decomposition of salts [14], solvothermal synthesis [15], "green method" [16, 17] etc. However, the using of usually toxic, dangerous precursors in the synthesis of magnetic nanoparticles significantly limits their biomedical applications. These circumstances have raised the demand for alternative reliable, non-toxic and environmentally friendly methods for the magnetite synthesis in order to extend its applications.

Among environmentally friendly "green" technologies, "green synthesis" with the use of plant or fruit extracts as precursors has become widespread. Plant extracts contain biologically active polyphenols, terpenoids, alcohols, carboxylic acids, amino acids, vitamin C, thiamine, ascorbic and oxalic acids, carbohydrates, etc. They are bioreducers of metals from solutions of their salts and participate in their further stabilization. The process of reducing the metal salt with plant extracts is very simple. The plant extract and the metal salt solution are mixed at room temperature. The reaction is complete within a few minutes. As soon as the solutions are mixed, the biochemical reduction of the salt begins immediately, and the formation of nanoparticles is usually manifested by a change in the solution color. Different parts of plants such as leaves, fruits, fruit skins, roots, seeds, etc. can be used for the synthesis. They contain phytochemicals such as flavonoids, xanthophylls, carotenoids, anthocyanins and phenolic compounds that are involved in the magnetite synthesis. Table 1 shows some characteristics of Fe_3O_4 nanoparticles obtained using different parts of plants. Extracts of various parts of grapes, such as leaves, stems, seeds and dried fruits, were used for the production of bimetallic nanoparticles Fe/Pd [24], Fe_3O_4-Ag [25] and silver [26] respectively. In [27], three different parts of grapes (seeds, peel and stalks) were used for the synthesis of gold nanoparticles.

Nanoparticles that exhibit magnetic properties have many applications in the medicine: magnetic resonance therapy, for cell separation, targeted drug delivery, magnetic hyperthermia, biochemical and immunological analysis of viruses, genes, antibodies etc. [28-35]. For *in vivo* biomedical applications, magnetic nanoparticles should be non-toxic with a particle size small enough to remain in circulation after injection and pass through the capillary systems of organs and tissues, avoiding vascular embolism. They must also be highly magnetized so that their movement in the blood can be controlled by a magnetic field and so that they can be immobilized near the target pathological tissue [36-39]. Hyperthermia is one of the newest treatments for cancer. In this method, target tissues or tumor cells were heated locally by various external sources [40]. According to the origin of heat, hyperthermia is divided into some types, such as electrical, optical and magnetic hyperthermia. The intensity of the heat generated and the accuracy of the heat targeting are two critical conditions for the performance of hyperthermia. Compared to other types of hyperthermia, magnetic ones shows more suitable conditions due to the sufficient amount of released heat and proper aiming accuracy. In magnetic hyperthermia, the nanoparticles are introduced into the body, and then move into the bloodstream and transferred to the tumors location under the applied magnetic field [41].

Moreover, magnetite (Fe_3O_4) has proven to be an effective Fenton-like catalyst that has been used successfully to degrade various contaminants in water [42, 43]. The Fenton-like reaction catalyzed by iron minerals is becoming an increasingly attractive option for the purification of groundwater contaminated with toxic organic substances. This process has a number of advantages, in particular: (i) iron minerals are able to catalyze the decomposition of H_2O_2 to form a hydroxyl radical (HO•) in a neutral pH medium; (ii) iron minerals are widespread in aquifers, which can initiate a Fenton-like reaction without prior preparation [44]; (iii) iron minerals and H_2O_2 are environmentally friendly materials for water treatment. Fe^{2+} ions, presented in the magnetite structure, promote the formation of active hydroxyl radicals HO•, so magnetite is more active in the Fenton-like reaction compared to other iron minerals, such as hematite, goethite and maghemite. However, the decomposition of H_2O_2 by Fe_3O_4 can sometimes pass through the non-radical mechanism with the formation of O_2 and H_2O. Therefore, there is an important problem of the synthesis of magnetite with an active surface, which will promote the radical decomposition of H_2O_2. Another important point is the use of environmentally safe concentration of H_2O_2. The high concentration of H_2O_2 ($\geq$ 250 mM) can threaten the safety of the environment. Thus, the aim of this work is to synthesize magnetite nanoparticles for magnetic hyperthermia application and H_2O_2 catalytic decomposition.

I. Experimental

1.1. Synthesis

The synthesis of magnetite nanoparticles performed by the auto-combustion method using reducing agents obtained from grape extract ("green" synthesis). Isabella hybrid grapes of two varieties *Vitis Labrusca* and *Vitis Vinifera* have been used. The fruits are divided into components: pulp and peel. Extracts of grape peel and pulp were prepared. They acted as reducing agents and stabilizing agents. The $Fe(NO_3)_3 \cdot 9H_2O$ was used as source of iron ions.

1.1.1. Preparation of grape extracts

Extract №1 (peel): 200 g of grape peels were filled with 350 mL of distilled water, heated and boiled for 30 minutes. The cooled peels extract was filtered through filter paper. The filtrate was used for further synthesis of magnetite nanoparticles.

Extract №2 (pulp): 300 g of grape pulp was added to 115 mL of distilled water, heated and boiled for 30 minutes. The cooled pulp extract was filtered through filter paper. The filtrate was used for further synthesis of magnetite nanoparticles.

1.1.2. Synthesis of magnetite

$Fe(NO_3)_3 \cdot H_2O$ (5.2 g) was dissolved in 50 mL of distilled water. The resulting solution was stirred with a magnetic stirrer for 30 minutes. 50 mL of grape extract was then added to the solution (grape peels extract was used for the synthesis of the Fe_3O_4-peel sample, and grape pulp extract was used for the synthesis of the Fe_3O_4-pulp sample). After adding the extracts, the solution changed its color from light yellow to dark brown. Stirring was continued on a magnetic stirrer for 30 minutes at 60 °C. After that, the solution was placed on a heating plate. It was observed that the solution turns into a sol, then into gel and there is an increase in viscosity. The ignition centers appear and auto-combustion occurs. The resulting powder was then washed with distilled water (60 °C) for five times and dried at room temperature.

1.2. Characterization methods

The phase composition of the samples was determined using an X-ray diffractometer with $Fe_{K\alpha}$ irradiation. The range of 2θ angles was from 20 to 130° with the scanning step of 0.05°. The phase amount and crystallite size were computed with the WinPLOTR software. The crystallite size (D) was computed according to the Scherrer formula:

$$D = \frac{K \cdot \lambda}{\beta \cdot \cos\theta}, \quad (1)$$

where D is average crystallite size; K is Scherrer constant (dimensionless particle shape factor, k = 0.92); λ is wavelength of X-rays (λ = 0.1936); β is peak width at half maximum (in radians); θ is diffraction angle (Bragg angle).

The morphology and elemental composition of the samples were examined using a REMMA scanning electron microscope with an attachment for energy-dispersive analysis. The accelerating voltage is approximately 20.00 kV.

Infrared spectra were recorded with a Specord M80 (Carl Zeiss, Germany) spectrophotometer in the range 400 – 4000 cm^{-1} (transmission mode). The samples were grinded with potassium bromide in the 1:100 ratio and pressed into pellets.

Mössbauer spectra were obtained with the MS1104Em spectrometer with moving absorber using $^{57}Co(Cr)$ radiation source. Spectra were recorded at room temperature in transmission geometry. The isomeric shift was calibrated accordingly to α-Fe. The velocity resolution was about 0.008 mm/s per channel. The resulting signal-to-noise ratios were greater than 31. The spectra were analyzed using UnivemMS 7.01 software.

1.3. Magnetic hyperthermia measurements

Induction heating of the magnetite samples was studied using induction coil (100 kHz, 1 kW, 5 cm in diameter). Water suspension of Fe_3O_4 samples was placed in induction coil made from cupper. The sample temperature was registered using an IR-thermometer. During the measurements, the induction coil was cooled by water to maintain a constant temperature of 20 ℃. Hyperthermia measurements for magnetite samples were performed during 40 minutes with step of 0.1 s. The dependence of the temperature change versus the heating time (electromagnetic field is on) and cooling time (electromagnetic field is off) was recorded. Changes of

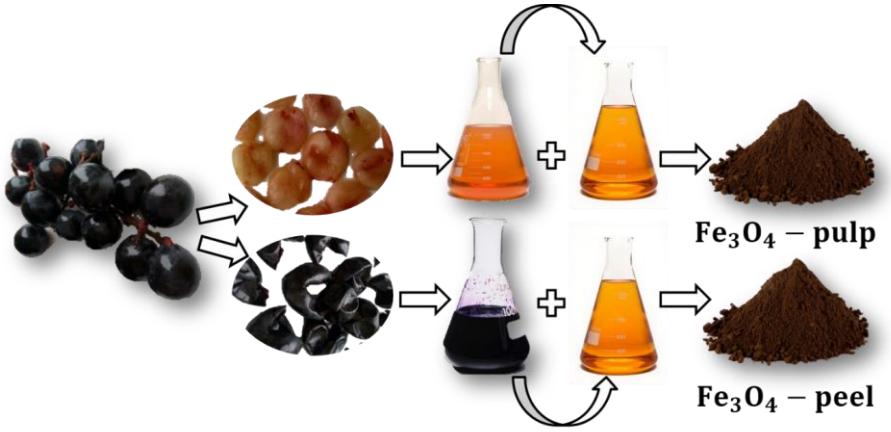

Fig. 1. The scheme of magnetite synthesis using grape peel and grape pulp extracts.

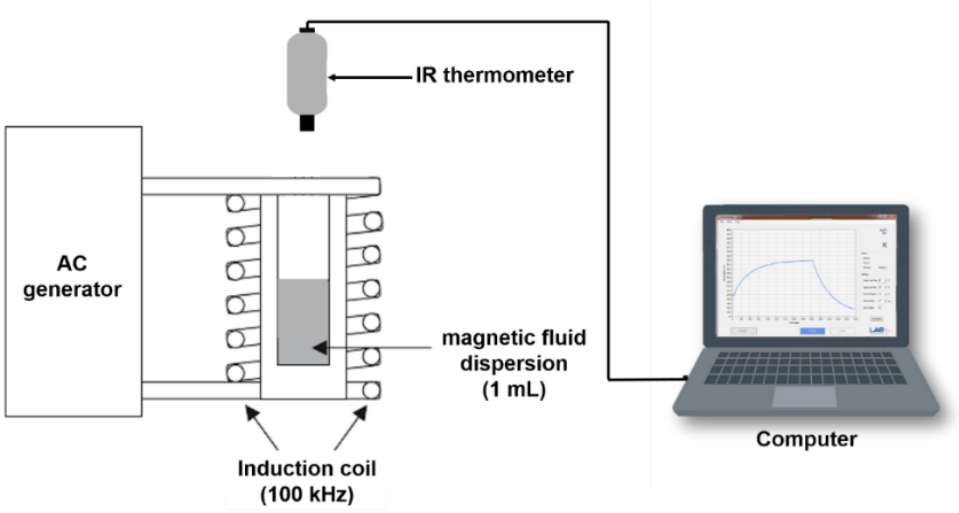

Fig. 2. Scheme of an induction heating experimental setup (cross-section).

temperature depending on sample concentration provide heating parameters important for magnetic hyperthermia applications.

1.4. Batch experiment for H_2O_2 decomposition

The catalytic processes were carried out in a batch reactor (100 cm^3) equipped with a stirrer (1000 rpm) in the presence of Fe_3O_4 catalysts. The catalyst concentration was 1 g/L and the hydrogen peroxide concentration was 5 mM. The experiments were performed at a temperature of 25 °C with continuous stirring for 120 minutes. The residual hydrogen peroxide concentration was determined by UV-spectroscopy at 240 nm (ULAB 102-UV spectrophotometer). The electrical conductivity was recorded using a conductometer Milwaukee Mi170, equipped with a conductometric sensor, and MI 5200 software. The redox potential was recorded using a laboratory pH meter PH800, equipped with an ORP electrode, and PCLink softwares. Both devices were simultaneously connected to a PC through USB ports.

II. Results and discussion

2.1. Structure characterization

The diffractograms of both magnetite samples, synthesized using extracts of grape peels and grape pulp (samples Fe_3O_4-peel and Fe_3O_4-pulp respectively) are shown in Fig. 3. Diffractograms indicate the formation of a single-phase cubic spinel. Peaks at angles 2θ = 38.45°, 45.40°, 55.50°, 69.40°, 74.25°, 82.15°, 126.10° indicate the formation of the spinel phase in both samples. The cubic spinel structure belongs to the space group Fd3m. The sample Fe_3O_4-peel has a lower crystallinity degree compared to Fe_3O_4-pulp sample. The value of the crystallite size (D) is equal to 7 nm for the Fe_3O_4-peel sample and 14 nm for the Fe_3O_4-pulp sample. The formation of nanosized particles was facilitated by mixing the starting reagents with grape extracts (acting as reducing and stabilizing agents). The calculations have shown that the crystallites size of magnetite sample, synthesized using grape pulp extract, is twice as big as the crystallites size of magnetite sample, synthesized using grape peel extract. This indicates a difference in the reducing ability of both grape extracts.

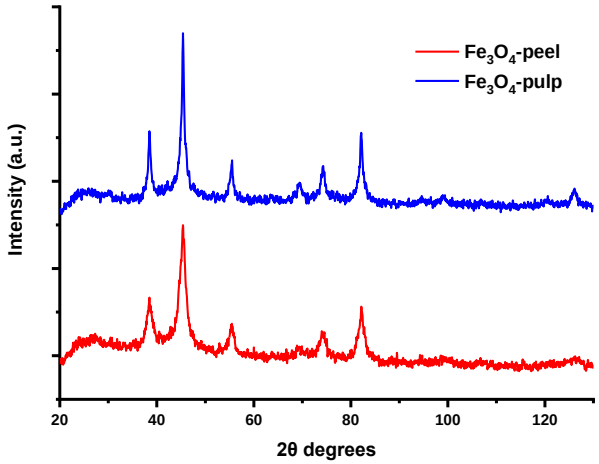

Fig. 3. The diffractograms of magnetite Fe_3O_4-peel and Fe_3O_4-pulp samples.

Crystalchemical parameters have been calculated using follow relations:

$$\rho_{XRD} = \frac{Z \cdot M}{N_A \cdot a^3}; \qquad r_{oct} = a\left(\frac{5}{8} - u\right) - R_O;$$
$$r_{tetr} = a\sqrt{3}\left(u - 0{,}25\right) - R_O \qquad (2)$$

where M is the molecular mass of the compound (g/mole), N_A is the Avogadro number ($6{,}023 \cdot 10^{23}$ $mole^{-1}$), Z is the number of atoms in the unit cell (Z = 8 for the compounds with a spinel structure), *a* is the lattice parameter (nm), *u* is the anionic parameter and R_O is the oxygen radius (0.138 nm). The structural parameters of the synthesized samples are given in Table 2.

Table 2.
Structural parameters of the Fe_3O_4-peel and Fe_3O_4-pulp magnetite samples.

Sample	*a* (Å)	V (Å^3)	*u*	ρ_{XRD} (g/cm^3)	D (nm)
Fe_3O_4-peel	8.3597	584.21	0.3754	5.264	7
Fe_3O_4-pulp	8.3555	583.33	0.3748	5.272	14

The morphology of the synthesized samples was examined using a scanning electron microscopy (Fig. 4). It is seen that the particles form agglomerates due to magnetic properties. The size of the agglomerates is in the nanometer range (< 100 nm). Energy-dispersive spectra of Fe_3O_4-peel and Fe_3O_4-pulp samples (Fig. 5) confirm the presence of Fe and O in the spinel structure. The experimental content of Fe and O coincides with the theoretically calculated one (Table 3).

Table 3.
The content of chemical elements in the synthesized magnetite samples.

Sample	Fe		O	
	at.% (theor.)	at.% (exp.)	at.% (theor.)	at.% (exp.)
Fe_3O_4-peel	43.86	41.24	57.14	58.76
Fe_3O_4-pulp	43.86	40.53	57.14	59.47

The analysis of the spinel structure also was carried out using IR spectroscopy. The obtained data presented in Fig. 6. The peak near 3400 cm^{-1} is related to adsorbed

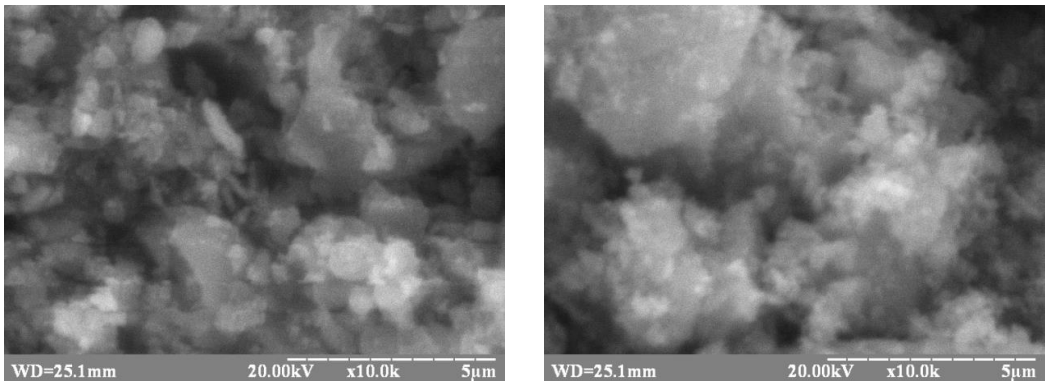

Fig. 4. Scanning electron microscopy images of Fe_3O_4-peel and Fe_3O_4-pulp samples.

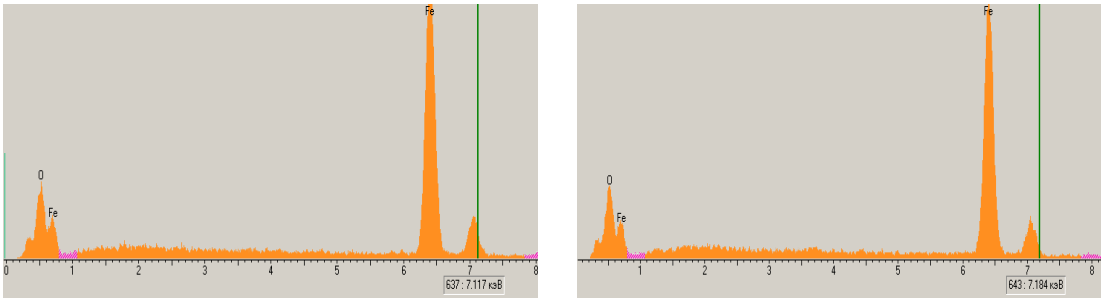

Fig. 5. Energy dispersive spectra of Fe_3O_4-peel and Fe_3O_4-pulp samples.

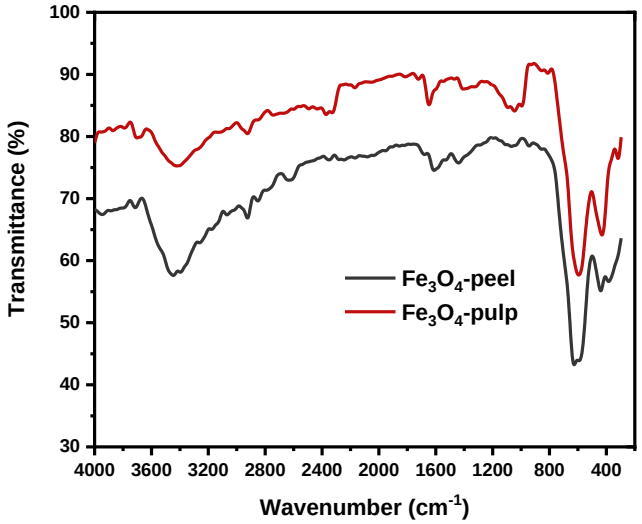

Fig. 6. IR spectra of magnetite samples, obtained using grape peel and grape pulp extracts.

water molecules. The peaks at ~1696 cm^{-1} for Fe_3O_4-pulp sample and ~1660 cm^{-1} for Fe_3O_4-peel sample are responsible for deformation vibrations of OH-bonds in the structure. Pronounced peaks at 596 cm^{-1} for Fe_3O_4-pulp sample and 602 cm^{-1} for Fe_3O_4-peel sample testify the vibration of tetrahedral Fe-O bonds, while peaks at 432 cm^{-1} for Fe_3O_4-pulp sample and 440 cm^{-1} for Fe_3O_4-peel sample testify the vibration of octahedral Fe-O bonds. Peaks at 1096 cm^{-1} and 1086 cm^{-1} correspond to stretching vibrations of NH_2-groups, which appeared from grape extracts and cause the functionalization of magnetite surface.

Debye temperature, θ_D, is related with many properties of solids, such as specific heat, electrical conductivity, thermal conductivity and elastic properties, and can be estimated using the following formula [45]:

$$\theta_D = \frac{h \cdot c \cdot \nu_{avg}}{k_B}, \quad (3)$$

where h is Planck constant (h = 6.62606957×10^{-34} J·s); c is light velocity (c=$3*10^{10}$ cm/s); $\nu_{avg} = \frac{(\nu_1 + \nu_2)}{2}$, ($\nu_1$ and ν_2 are peak frequencies of the M–O bonds of the octahedral and tetrahedral sites, respectively); k_B is Boltzmann constant (1.380649×10^{-23} J/K). The calculated values of Debye temperature are 750 K and 740 K for Fe_3O_4-peel and Fe_3O_4-pulp samples respectively (Table 4).

Table 4.

Wavenumbers of the IR absorption bands for the magnetite samples.

Sample	ν_1 (cm^{-1}) (B-site)	ν_2 (cm^{-1}) (A-site)	ν_{avg}	θ_D (K)
Fe_3O_4-peel	440	602	521	750
Fe_3O_4-pulp	432	596	514	740

2.2. Mössbauer studies

Room-temperature Mössbauer spectra of Fe_3O_4-peel and Fe_3O_4-pulp samples are shown in Fig. 7. The superparamagnetic relaxation is the main factor determining the spectra. Both spectra exhibit broad magnetically splitted component and central paramagnetic doublet. The observed compositions correspond to the presence of ferrimagnetic particles in an intermediate state between magnetically ordered and paramagnetic ordered due to the proximity of Neel relaxation time τ_N of a certain particle and the measurement time τ_m (lifetime of ^{57}Fe nucleus excited state, τ_m=141.8 ns). The Neel time can be calculated as $\tau_N = \tau_0 \exp(\frac{K_{eff} V}{kT})$, where τ_0 is the characteristic of a material ($\tau_0 \approx 10^{-9}$c) [46], K_{eff} is an effective magnetocrystalline anisotropy constant, V is a volume of a nanoparticle, T is a temperature. It is clear that the condition of ferrimagnetic-paramagnetic transition at constant temperature is determined by both particle size and effective magnetocrystalline anisotropy constant, which is also size-sensitive due to the increasing of surface anisotropy contribution. The detailed analysis of the spectra is complicated by the presence of particle size distribution. However, using the value $K_{eff} = 1.7\times10^4$ J/m³ of effective magnetic anisotropy of the magnetite nanoparticles with averaged size 10 nm [47], we get the proximity of τ_N and τ_m values. The relative content of paramagnetic component is observed for Fe_3O_4-peel sample that correspond to XRD data and average particle size.

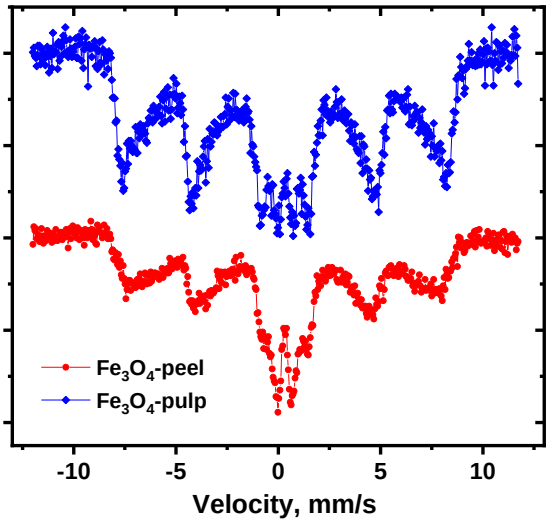

Fig. 7. Room temperature Mossbauer spectra of Fe_3O_4-peel and Fe_3O_4-pulp samples.

2.3. Hyperthermic parameters

Magnetic hyperthermia is a treatment method that involves the selective destruction of tumor cells without damaging the surrounding tissues [48]. Cancerous tissues do not have a developed vascular system, thus their thermal resistance is greater than that of healthy tissues, so they cannot be effectively cooled. Tumor cells heated to about 42 °C begin to die, while healthy cells remain largely intact up to 48 °C [49, 50]. A long-time thermal impact causes the death of cancer cells. It can be through two mechanisms: apoptosis and necrosis. Unlike necrosis, apoptosis is a natural non-toxic sequential cell death. It is known that necrosis occurs at higher temperatures than apoptosis [51]. Based on numerous studies, the temperature of 43 °C is accepted as the maximal safe temperature for hyperthermia treatment [48, 52]. The degree and rate of heating depends on the size, shape, chemical composition, concentration of the magnetic nanoparticles, as well as the viscosity of the medium in which the magnetic nanoparticles are dissolved, and frequency of the applied magnetic field [11, 53]. The hyperthermia curves for Fe_3O_4-peel and Fe_3O_4-pulp samples are shown in Fig. 8a and 8c, respectively.

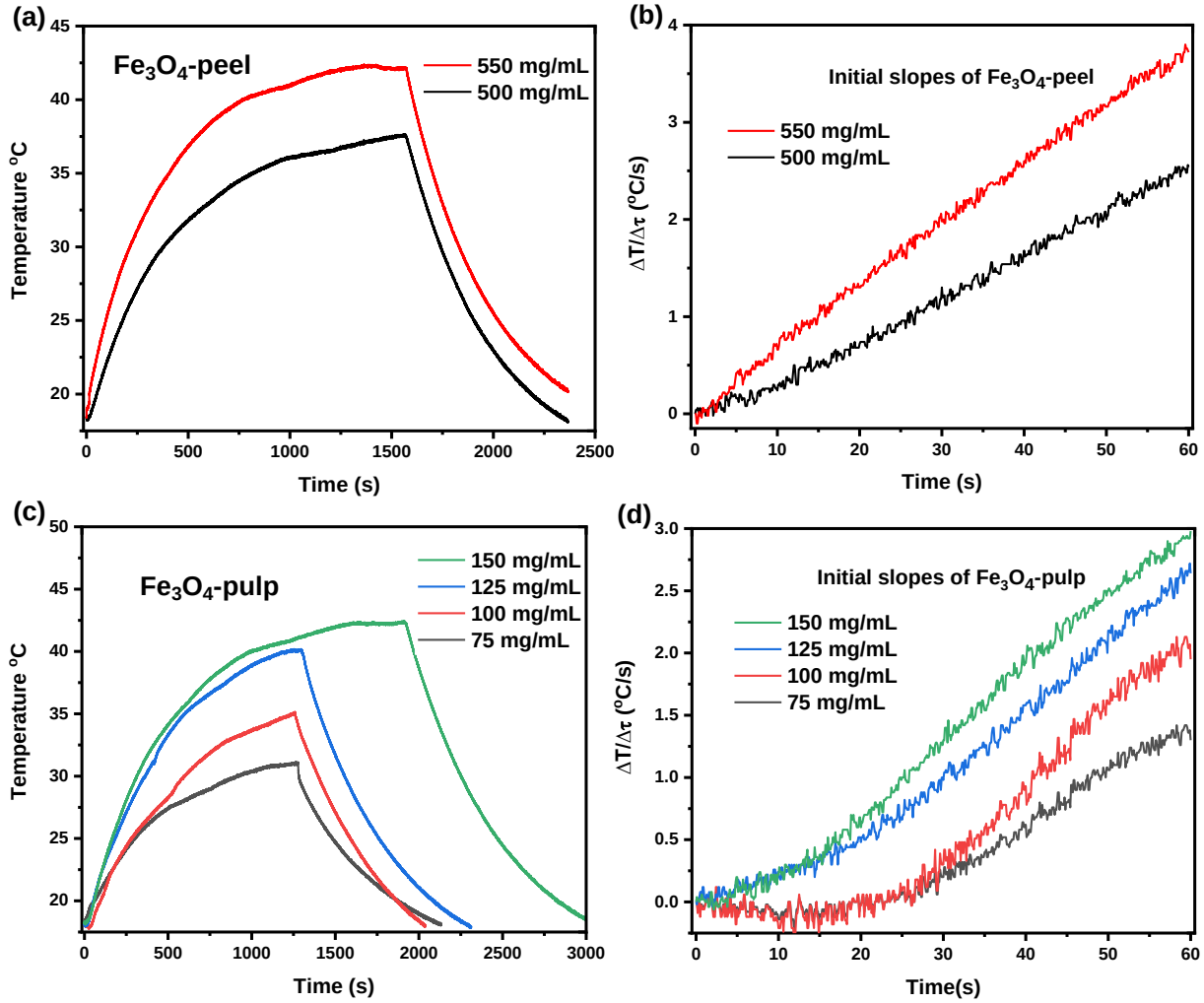

Fig. 8. Magnetic hyperthermia measurements: (a) induction heating curves of Fe_3O_4-peel suspension in water; (b) initial slopes of the temperature change curves versus time for Fe_3O_4-peel sample; (c) induction heating curves of Fe_3O_4-pulp suspension in water; (d) initial slopes of the temperature change curves versus time for Fe_3O_4-pulp sample.

The heating efficiency of magnetic nanoparticles is characterized by specific absorption rate (SAR) what is defined as the amount of energy that is converted into heat over time per certain mass [54-56]. SAR (in W/g) is calculated based on the initial linear increase in temperature ΔT over a time interval Δτ:

$$\mathrm{SAR}\left(\frac{\mathrm{W}}{\mathrm{g}}\right)=\frac{\mathrm{c}}{\mathrm{m}}\times\frac{\Delta\mathrm{T}}{\Delta\tau}, \qquad (4)$$

where c is specific heat capacity of water (4185 J/K) and m (g/L) is the mass of magnetic sample, dispersed in the aqueous medium. The slope ΔT/Δτ was calculated for the first 60 s (Fig. 8b, Fig. 8d). The SAR values are presented in Table 5. The obtained SAR values for Fe_3O_4-peel and Fe_3O_4-pulp magnetic nanoparticles show the potential for their use in magnetic hyperthermia applications. The data are in agreement with literature [57]. The increase of SAR values could be reached by increasing of induction coil frequency [11].

Table 5.
SAR values for magnetite samples, obtained using grape peel and grape pulp extracts.

Sample	Mass of the sample (mg)	Final temp. T_f (°C)	Slopes ΔT/Δτ (°C/s)	SAR (W/g)
Fe_3O_4-peel	500	37.51	0.0408	0.341
	550	42.28	0.0642	0.488
Fe_3O_4-pulp	75	30.90	0.0168	0.937
	100	35.06	0.0253	1.058
	125	39.95	0.0393	1.315
	150	42.48	0.0477	1.330

2.4. Catalytic activity

Fig. 9 shows the catalytic activity of magnetite samples, obtained using grape peel (Fe_3O_4-peel) and grape pulp (Fe_3O_4-pulp) extracts. Fig. 9a presents the degree of H_2O_2 decomposition *vs.* reaction time in the presence of magnetite catalysts at 298 K. According to the obtained results, the samples showed almost the same activity. A Fe_3O_4-peel sample is slightly more active: a degree of decomposition of hydrogen peroxide is 67.5 % within 120 minutes, while a Fe_3O_4-pulp sample showed a degree of hydrogen peroxide decomposition of 65.25 % during the same conditions. The logarithmic kinetic curves are presented in Fig. 9b. They indicate that the experimental data are well described by the first-order kinetic model (the values of R^2 are 0.9157 and 0.9380). Fig. 10 presents the UV-Vis spectra in the wavelength range from 200 to 340 nm of the residual H_2O_2 in the solutions at the presence of Fe_3O_4-peel (Fig. 10a) and Fe_3O_4-pulp (Fig. 10b) catalysts.

The electrical conductivity of the H_2O_2 solutions in the presence of Fe_3O_4-peel and Fe_3O_4-pulp catalysts was measured using an ORP sensor and depicted in Fig. 11a. Fig. 11b shows the redox potential of the H_2O_2 solutions *vs.* time in the presence of Fe_3O_4-peel and Fe_3O_4-pulp catalysts. The change in electrical conductivity and ORP is caused probably by OH^-, Fe^{2+} and Fe^{3+} ions, •OH, $O_2^{\bullet-}$ and HO_2• radicals [58], formed during the catalytic decomposition of H_2O_2:

$$Fe^{3+} + H_2O_2 \rightarrow Fe^{2+} + 2H^+ + O_2^{\bullet-} \quad (5)$$

$$Fe^{3+} + O_2^{\bullet-} \rightarrow Fe^{2+} + O_2 \quad (6)$$

$$Fe^{2+} + H_2O_2 \rightarrow Fe^{3+} + HO^{\bullet} + OH^- \quad (7)$$

The formed radicals react with a wide range of organic pollutants (dyes, phenols and pharmaceuticals) and cause their destruction [59]. As can be seen from Fig. 11a, the conductivity is increased for both magnetite catalysts due to accelerated formation of radicals from hydrogen peroxides molecules.

The oxidation-reduction potential (ORP) is other water quality parameter and its recording can be used as "real-time" monitoring of water disinfection potential

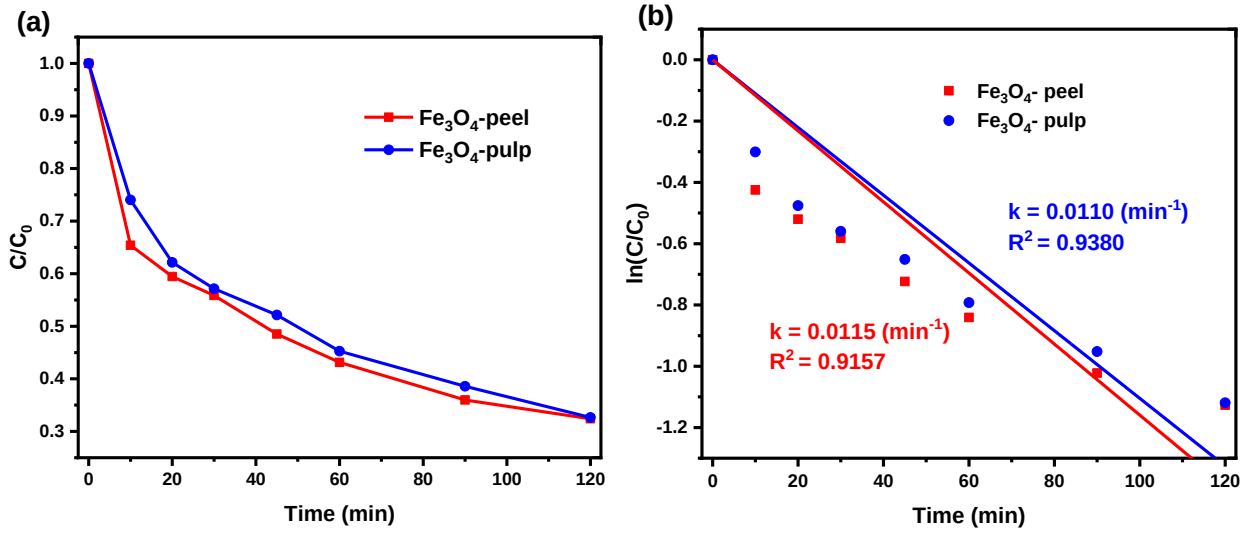

Fig. 9. Catalytic activity of magnetite samples, obtained using grape peel (Fe_3O_4-peel) and grape pulp (Fe_3O_4-pulp) extracts: (a) degree of H_2O_2 decomposition *vs.* reaction time in the presence of magnetite catalysts at 298 K; (b) first-order model for magnetite catalysts at 298 K.

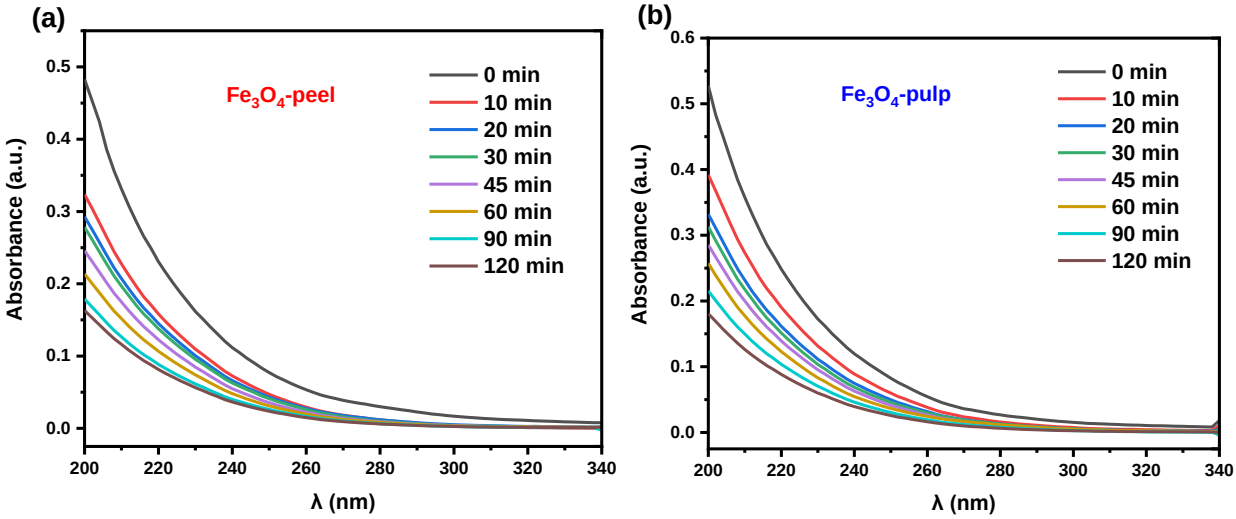

Fig. 10. UV-Vis spectra of the residual H_2O_2 in the solutions at the presence of catalysts: (a) Fe_3O_4-peel; (b) Fe_3O_4-pulp.

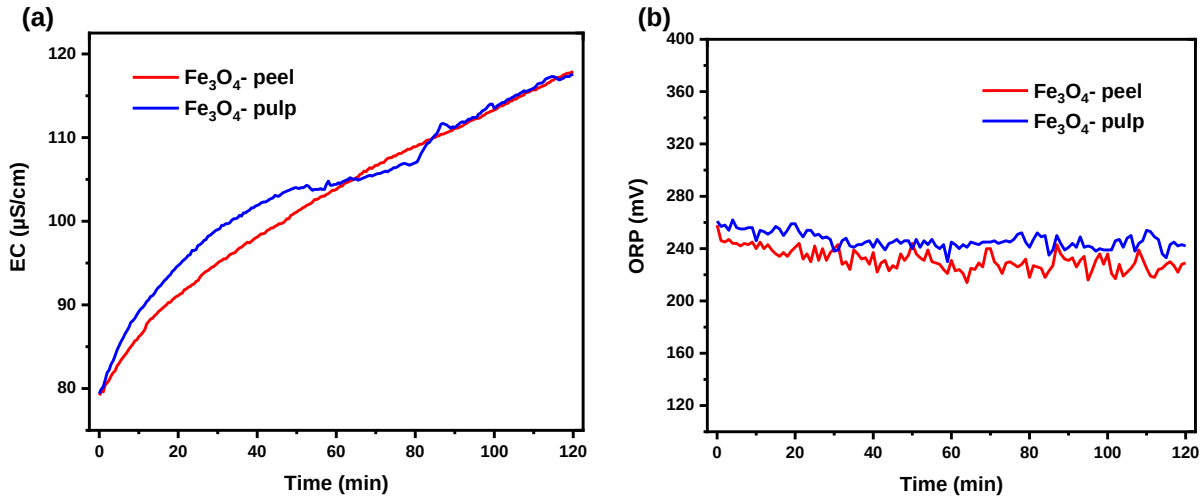

Fig. 11. (a) Electrical conductivity of the H_2O_2 solutions in the presence of Fe_3O_4-peel and Fe_3O_4-pulp catalysts at 298 K; (b) Oxidation-reduction potential (ORP) of the H_2O_2 solutions in the presence of Fe_3O_4-peel and Fe_3O_4-pulp catalysts at 298 K.

[60,61]. The ORP measurements showed that the ORP curves (Fig. 11b) have tendency to decrease for both magnetite catalysts. In the first 40 minutes the ORP decreased from 258 mV to 235 mV for catalytic process in the presence of Fe_3O_4-peel sample and from 261 mV to 245 mV for catalytic process in the presence of Fe_3O_4-pulp sample and then remain almost constant for next 80 minutes. It can be explained by constant formation of hydroxyl radicals due to Fenton mechanism. Thus, the studied magnetite nanocatalysts have potential for their application in water treatment.

Conclusions

Magnetite nanoparticles were synthesized by the "green" chemistry method using the reducing agents, obtained from grape extracts (peels and pulp). X-ray analysis confirmed the formation of a single-phase spinel structure. Based on the obtained data, the crystal chemical parameters of the synthesized magnetite samples were calculated. The sizes of the crystallites are in the nanometer range (7 nm for the Fe_3O_4-peel sample and 14 nm for the Fe_3O_4-pulp). The anion parameters *u* are 0.3754 nm and 0.3748 nm for Fe_3O_4-peel and Fe_3O_4-pulp samples, respectively. It was found that the SAR values increases linearly with increasing of concentration of magnetic nanoparticles in the suspensions. The SAR values are 0.488 W/g and 1.330 W/g for Fe_3O_4-peel and Fe_3O_4-pulp samples, respectively. Studies of the catalytic activity of the synthesized magnetite nanoparticles were performed using a batch reactor equipped with a conductometry sensor and an ORP electrode. The kinetic curves fit with first-order kinetic model. The rate constants are 0.0110 min^{-1} and 0.0115 min^{-1} for the Fe_3O_4-peel and Fe_3O_4-pulp samples, respectively. The samples demonstrate good catalytic activity towards the H_2O_2 removal from wastewater.

Acknowledgment

The authors thank the Ministry of Education and Science of Ukraine for financial support in the framework of project number 0121U109476 ("Engineering of metal oxide catalysts with the regulating activity function for hydroxyradical water disinfection", 2021-2023).

Danyliuk N. **–** PhD student, leading specialist at the Educational and Scientific Center of Material Science and Nanotechnology;
Lischynska S. **–** Master student;
Tatarchuk T. – Associate Professor of the Chemistry Department, Director of Educational and Scientific Center of Materials Science and Nanotechnology;
Kotsyubynsky V. – Doctor of Physical and Mathematical Sciences;
Mandzyuk V. – Associate Professor of the Department of Computer Engineering and Electronics.

[1] P. Legutko, W. Kaspera, P. Stelmachowski, Z. Sojka, A. Kotarba, Catal. Commun. 56, 139 (2014); https://doi.org/10.1016/J.CATCOM.2014.07.020.
[2] A. Dhakshinamoorthy, S. Navalon, M. Alvaro, Chem. Sus. Chem. 5, 46 (2012); https://doi.org/10.1002/cssc.201100517.
[3] M. Arakha, S. Pal, D. Samantarrai, T.K. Panigrahi, B.C. Mallick, K. Pramanik, B. Mallick, S. Jha, Sci. Rep. 5, 1 (2015); https://doi.org/10.1038/srep14813.
[4] A.R. Yasemian, M. Almasi Kashi, A. Ramazani, Mater. Chem. Phys. 230, 9 (2019); https://doi.org/10.1016/j.matchemphys.2019.03.032.
[5] C.F. Carolin, P.S. Kumar, A. Saravanan, G.J. Joshiba, M. Naushad, J. Environ. Chem. Eng. 5, 2782 (2017); https://doi.org/10.1016/J.JECE.2017.05.029.

[6] J. Gómez-Pastora, S. Dominguez, E. Bringas, M.J. Rivero, I. Ortiz, Chem. Eng. J. 310, 407 (2017); https://doi.org/10.1016/J.CEJ.2016.04.140.
[7] D.H.K. Reddy, Y.S. Yun, Coord. Chem. Rev. 315, 90 (2016); https://doi.org/10.1016/j.ccr.2016.01.012.
[8] X. Hou, X. Wang, W. Mi, J. Alloys Compd. 765, 1127 (2018); https://doi.org/10.1016/J.JALLCOM.2018.06.287.
[9] M. Amiri, M. Salavati-Niasari, A. Akbari, Adv. Colloid Interface Sci. 265, 29 (2019); https://doi.org/10.1016/J.CIS.2019.01.003.
[10] C. Bárcena, A.K. Sra, J. Gao, Nanoscale Magn. Mater. Appl. 167, 591 (2009); https://doi.org/10.1007/978-0-387-85600-1_20.
[11] V. Kusigerski, E. Illes, J. Blanusa, S. Gyergyek, M. Boskovic, M. Perovic, V. Spasojevic, J. Magn. Magn. Mater. 475, 470 (2018); https://doi.org/10.1016/j.jmmm.2018.11.127.
[12] O. Lemine, K. Omri, B. Zhang, Superlattices Microstruct. 52(4), 793 (2012); https://doi.org/10.1016/j.spmi.2012.07.009.
[13] Z.L. Liu, X. Wang, K.L. Yao, G.H. Du, Q.H. Lu, Z.H. Ding, J. Tao, Q. Ning, X.P. Luo, D.Y. Tian, D. Xi, J. Mater. Sci. 39, 2633 (2004); https://doi.org/10.1023/B:JMSC.0000020046.68106.22.
[14] N.R. Jana, Y. Chen, X. Peng, Chem. Mater. 16, 3931 (2004); https://doi.org/10.1021/cm049221k.
[15] X. Wang, J. Zhuang, Q. Peng, Y. Li, Nature 437; 121 (2005); https://doi.org/10.1038/nature03968.
[16] F. Buazar, M.H. Baghlani-Nejazd, M. Badri, M. Kashisaz, A. Khaledi-Nasab, F. Kroushawi, Starch/Staerke 68, 796 (2016); https://doi.org/10.1002/star.201500347.
[17] R. Rahmani, M. Gharanfoli, M. Gholamin, M. Darroudi, J. Chamani, K. Sadri, J. Mol. Struct. 1196, 394 (2019); https://doi.org/10.1016/j.molstruc.2019.06.076.
[18] Y. Cai, Y. Shen, A. Xie, S. Li, X. Wang, J. Magn. Magn. Mater. 322, 2938 (2010); https://doi.org/10.1016/j.jmmm.2010.05.009.
[19] S. Phumying, S. Labuayai, C. Thomas, V. Amornkitbamrung, E. Swatsitang, S. Maensiri, Appl. Phys. A Mater. Sci. Process. 111, 1187 (2013); https://doi.org/10.1007/s00339-012-7340-5.
[20] S. Narayanan, B.N. Sathy, U. Mony, M. Koyakutty, S. V. Nair, D. Menon, ACS Appl. Mater. Interfaces. 4, 251 (2012); https://doi.org/10.1021/am201311c.
[21] N. Latha, M. Gowri, Int. J. Sci. Res. 3, 1551 (2014); https://doi.org/10.1380/ejssnt.2014.363.
[22] L. Xiao, M. Mertens, L. Wortmann, S. Kremer, M. Valldor, T. Lammers, F. Kiessling, S. Mathur, ACS Appl. Mater. Interfaces. 7, 6530 (2015); https://doi.org/10.1021/am508404t.
[23] A. Bahadur, A. Saeed, M. Shoaib, S. Iqbal, M.I. Bashir, M. Waqas, M.N. Hussain, N. Abbas, Mater. Chem. Phys. 198, 229 (2017); https://doi.org/10.1016/j.matchemphys.2017.05.061.
[24] F. Luo, D. Yang, Z. Chen, M. Megharaj, R. Naidu, Sci. Total Environ. 562, 526 (2016); https://doi.org/10.1016/j.scitotenv.2016.04.060.
[25] S. Venkateswarlu, B. Natesh Kumar, B. Prathima, K. Anitha, N.V.V. Jyothi, Phys. B Condens. Matter. 457; 30 (2015); https://doi.org/10.1016/j.physb.2014.09.007.
[26] J. Bastos-Arrieta, A. Florido, C. Pérez-Ràfols, N. Serrano, N. Fiol, J. Poch, I. Villaescusa, Nanomaterials 8, 946 (2018); https://doi.org/10.3390/nano8110946.
[27] K. Krishnaswamy, H. Vali, V. Orsat, J. Food Eng. 142, 210 (2014); https://doi.org/10.1016/j.jfoodeng.2014.06.014.
[28] S. Sukumaran, N. Ms, N. Shaji, JSM Nanotechnol. Nanomedicine 6, 1068 (2018).
[29] G. Kandasamy, D. Maity, Int. J. Pharm. 496, 191 (2015); https://doi.org/10.1016/j.ijpharm.2015.10.058.
[30] K. McNamara, S.A.M. Tofail, Adv. Phys. X. 2, 54 (2017); https://doi.org/10.1080/23746149.2016.1254570.
[31] T.E. Torres, M.R. Ibarra, G.F. Goya, Colloids Surfaces B Biointerfaces. 6, 2008 (2009); https://doi.org/10.1016/j.colsurfb.2018.02.031.
[32] M.T.H. Bhuiyan, M.N. Chowdhury, M.S. Parvin, ARC J. Cancer Sci. 2, 25 (2016); https://doi.org/10.20431/2455-6009.0202004.
[33] Y.T. Chen, A.G. Kolhatkar, O. Zenasni, S. Xu, T.R. Lee, Biosensing using magnetic particle detection techniques (2017); https://doi.org/10.3390/s17102300.
[34] Y. Chen, X. Ding, Y. Zhang, A. Natalia, X. Sun, Z. Wang, H. Shao, Quant. Imaging Med. Surg. 8, 957 (2018); https://doi.org/10.21037/qims.2018.10.07.
[35] K. McNamara, S.A.M. Tofail, Phys. Chem. Chem. Phys. 17, 27981 (2015) https://doi.org/10.1039/c5cp00831j.
[36] D.L.J. Thorek, A.K. Chen, J. Czupryna, A. Tsourkas, Ann. Biomed. Eng. 34, 23 (2006); https://doi.org/10.1007/s10439-005-9002-7.
[37] M.A. López-Quintela, C. Tojo, M.C. Blanco, L. García Rio, J.R. Leis, Curr. Opin. Colloid Interface Sci. 9, 264 (2004); https://doi.org/10.1016/j.cocis.2004.05.029.
[38] P. Ayyub, M. Multani, M. Barma, V.R. Palkar, R. Vijayaraghavan, J. Phys. C Solid State Phys. 21, 2229 (1988); https://doi.org/10.1088/0022-3719/21/11/014.
[39] N. Danyliuk, J. Tomaszewska, T. Tatarchuk, J. Mol. Liq. 309, 113077 (2020); https://doi.org/10.1016/j.molliq.2020.113077.
[40] S. Laurent, S. Dutz, U.O. Häfeli, M. Mahmoudi, Adv. Colloid Interface Sci. 166, 8 (2011); https://doi.org/10.1016/j.cis.2011.04.003.

[41] M. Mahmoudi, P. Stroeve, A.S. Milani, A.S. Arbab, Nov. Sci. Publ. 1 (2011).
[42] N. Wang, D. Jia, Y. Jin, S. Sun, Q. Ke, Environ. Sci. Pollut. Res. 24, 17598 (2017); https://doi.org/10.1007/s11356-017-9387-5.
[43] L. Hu, P. Wang, G. Liu, G. Zhang, Chemosphere 240; 124977 (2020); https://doi.org/10.1016/j.chemosphere.2019.124977.
[44] A.L. Pham, F.M. Doyle, D.L. Sedlak, Water Res. 46, 6454 (2012); https://doi.org/10.1016/j.watres.2012.09.020.
[45] T. Tatarchuk, M. Bououdina, W. Macyk, O. Shyichuk, N. Paliychuk, I. Yaremiy, B. Al-Najar, M. Pacia, Nanoscale Res. Lett. 12, (2017); https://doi.org/10.1186/s11671-017-1899-x.
[46] V.O. Kotsyubynsky, V. V. Moklyak, A.B. Hrubiak, Mater. Sci. Pol. 32, 481 (2014); https://doi.org/10.2478/s13536-014-0202-4.
[47] G.B. Oliveira-Filho, J.J. Atoche-Medrano, F.F.H. Aragón, J.C. Mantilla Ochoa, D.G. Pacheco-Salazar, S.W. da Silva, J.A.H. Coaquira, Appl. Surf. Sci. 563, 1 (2021); https://doi.org/10.1016/j.apsusc.2021.150290.
[48] Z. Hedayatnasab, F. Abnisa, W.M.A.W. Daud, Mater. Des. 123, 174 (2017); https://doi.org/10.1016/j.matdes.2017.03.036.
[49] M. Srivastava, S.K. Alla, S.S. Meena, N. Gupta, R.K. Mandal, N.K. Prasad, Ceram. Int. 45, 12028 (2019); https://doi.org/10.1016/j.ceramint.2019.03.097.
[50] E.C. Abenojar, S. Wickramasinghe, J. Bas-Concepcion, A.C.S. Samia, Prog. Nat. Sci. Mater. Int. 26, 440 (2016); https://doi.org/10.1016/j.pnsc.2016.09.004.
[51] F. Gao, Y. Cai, J. Zhou, X. Xie, W. Ouyang, Y. Zhang, X. Wang, X. Zhang, X. Wang, L. Zhao, J. Tang, Nano Res. 3, 23 (2010); https://doi.org/10.1007/s12274-010-1004-6.
[52] A. Hanini, K. Kacem, J. Gavard, H. Abdelmelek, S. Ammar, Elsevier Inc., 2018; https://doi.org/10.1016/B978-0-12-813351-4.00036-5.
[53] A.B. Salunkhe, V.M. Khot, S.H. Pawar, Curr. Top. Med. Chem. 14, 572 (2014); https://doi.org/10.2174/1568026614666140118203550.
[54] S. Mondal, P. Manivasagan, S. Bharathiraja, M.S. Moorthy, V.T. Nguyen, H.H. Kim, S.Y. Nam, K.D. Lee, J. Oh, Nanomaterials 7, 1 (2017); https://doi.org/10.3390/nano7120426.
[55] T. Tatarchuk, A. Shyichuk, Z. Sojka, J. Gryboś, M. Naushad, V. Kotsyubynsky, M. Kowalska, S. Kwiatkowska-Marks, N. Danyliuk, J. Mol. Liq. 328, 115375 (2021); https://doi.org/10.1016/j.molliq.2021.115375.
[56] T. Tatarchuk, M. Myslin, I. Lapchuk, O. Olkhovyy, N. Danyliuk, V. Mandzyuk, Phys. Chem. Solid State. 22, 195 (2021); https://doi.org/10.15330/pcss.22.2.195-203.
[57] R.R. Shah, T.P. Davis, A.L. Glover, D.E. Nikles, C.S. Brazel, J. Magn. Magn. Mater. 387, 96 (2015); https://doi.org/10.1016/j.jmmm.2015.03.085.
[58] M.Z. Wei Wang, Qiong Mao, Huanhuan He, Water Sci Technol. 68, 2367 (2013); https://doi.org/10.2166/wst.2013.497.
[59] N. Jaafarzadeh, A. Takdastan, S. Jorfi, F. Ghanbari, M. Ahmadi, G. Barzegar, J. Mol. Liq. 256, 462 (2018); https://doi.org/10.1016/j.molliq.2018.02.047.
[60] C.-H. Lin, R.-F. Yu, W.-P. Cheng, C.-R. Liu, J. Hazard. Mater. 209–210, 348 (2012); https://doi.org/10.1016/j.jhazmat.2012.01.029.
[61] R.-F. Yu, Chemosphere. 56, 973 (2004); https://doi.org/10.1016/j.chemosphere.2004.03.015.

Н. Данилюк, С. Ліщинська, Т. Татарчук, В. Коцюбинський, В. Мандзюк

Синтез наночастинок магнетиту з використанням екстракту винограду: синтез, морфологія, застосування в гіпертермії та каталітична активність у реакції розкладу пероксиду водню

Прикарпатський національний університет імені Василя Стефаника, Івано-Франківськ, Україна, danyliuk.nazariy@gmail.com

У статті представлено простий одноетапний "зелений" підхід до синтезу наночастинок магнетиту. Наночастинки магнетиту синтезовані з використанням екстрактів винограду, отриманих зі шкірок та м'якоті. Утворення наночастинок магнетиту було підтверджено за допомогою Х-променевої дифракції, інфрачервоної спектроскопії (ІЧ), мессбауерівської спектроскопії, скануючої електронної мікроскопії (СЕМ) та енергодисперсійної спектроскопії (ЕДС). Розмір кристалітів наночастинок магнетиту становив 7 і 14 нм для зразків Fe_3O_4-шкірка та Fe_3O_4-м'якоть відповідно. Синтезовані наночастинки магнетиту показали перспективи їх використання у магнітній гіпертермії. Значення питомої швидкості поглинання електромагнітної енергії дорівнюють 0.488 Вт/г та 1.330 Вт/г для зразків Fe_3O_4-шкірка та Fe_3O_4-м'якоть відповідно. Максимальні температури гіпертермії становлять 42.28 °С і 42.48 °С для зразків Fe_3O_4-шкірка та Fe_3O_4-м'якоть відповідно. Каталітичну активність магнетиту досліджували в реакції розкладу пероксиду водню в реакторі періодичної дії. Висока каталітична активність синтезованих зразків робить їх перспективними каталізаторами розкладу пероксиду водню в технологіях очищення води.

Ключові слова: зелений синтез, магнетит, магнітна гіпертермія, каталітична активність, пероксид водню.